

# DocXplain: A Novel Model-Agnostic Explainability Method for Document Image Classification\*

Saifullah Saifullah<sup>1,2</sup>[0000–0003–3098–2458], Stefan Agne<sup>1,3</sup>[0000–0002–9697–4285],  
Andreas Dengel<sup>1,2</sup>[0000–0002–6100–8255], and Sheraz  
Ahmed<sup>1,3</sup>[0000–0002–4239–6520]

<sup>1</sup> Smarte Daten and Wissensdienste (SDS), Deutsches Forschungszentrum für Künstliche Intelligenz GmbH (DFKI), Trippstadter Straße 122, 67663 Kaiserslautern, Germany

{firstname.lastname}@dfki.de

<sup>2</sup> Department of Computer Science, RPTU Kaiserslautern-Landau, Erwin-Schrödinger-Straße 52, 67663 Kaiserslautern, Germany

<sup>3</sup> DeepReader GmbH, 67663 Kaiserslautern, Germany

**Abstract.** Deep learning (DL) has revolutionized the field of document image analysis, showcasing superhuman performance across a diverse set of tasks. However, the inherent black-box nature of deep learning models still presents a significant challenge to their safe and robust deployment in industry. Regrettably, while a plethora of research has been dedicated in recent years to the development of DL-powered document analysis systems, research addressing their transparency aspects has been relatively scarce. In this paper, we aim to bridge this research gap by introducing DocXplain, a novel model-agnostic explainability method specifically designed for generating high interpretability feature attribution maps for the task of document image classification. In particular, our approach involves independently segmenting the foreground and background features of the documents into different document elements and then ablating these elements to assign feature importance. We extensively evaluate our proposed approach in the context of document image classification, utilizing 4 different evaluation metrics, 2 widely recognized document benchmark datasets, and 10 state-of-the-art document image classification models. By conducting a thorough quantitative and qualitative analysis against 9 existing state-of-the-art attribution methods, we demonstrate the superiority of our approach in terms of both faithfulness and interpretability. To the best of the authors' knowledge, this work presents the first model-agnostic attribution-based explainability method specifically tailored for document images. We anticipate that our work will significantly contribute to advancing research on transparency, fairness, and robustness of document image classification models.

**Keywords:** Explainable Document Classification · Explainable AI Document Image Classification · Model Interpretability · Model-Agnostic

---

\* This work was supported by the BMBF projects SensAI (BMBF Grant 01IW20007)

## 1 Introduction

The recent breakthroughs in deep learning (DL) have ignited a revolution in the field of document analysis, leading to noteworthy progress in a wide variety of document understanding tasks [2,8,40,19,45,34]. However, the inherent lack of transparency in black-box DL models continues to raise questions about their suitability for real-world applications [56,38,57]. Numerous recent studies [31,10,27,16,38] have shown that DL-based automated decision-making systems can easily succumb to data biases [31,10,27,16], which may lead to incorrect decision-making [56,38] or discrimination against individuals of minority groups [46,57]. One such decision-making process is automated document image classification [2,8,40,19], which may appear harmless at first but harbors the potential to become a source of great unfairness in specific scenarios—such as the unfair or biased rejection of applicant resumes from minority groups due to hidden biases present in the data.

Besides the lack of transparency, deep learning models are also well-known for their vulnerability to minor data perturbations [6] and out-of-distribution (OOD) data [14,39]. This raises questions about their robustness and underscores the necessity for an explainability framework that could be utilized to trace and validate model behavior before deployment in real-world applications. This requirement is especially crucial in the context of intelligent document processing, given that business documents encountered in real-world settings are not only typically corrupted with novel degradations [39,35] but also frequently appear in various novel layouts, featuring content that was unseen during the training phase [12,24,33]. Such OOD data samples may lead to failures at test time, making the traceability of decisions important for determining the reasons behind such failures.

The field of eXplainable AI (XAI) [7,36] has recently emerged to address the aforementioned issues of transparency and accountability, with numerous methods proposed in recent years [37,44,50,29,49,30] that attempt to explain the predictions of black-box DL models. However, despite significant attention devoted to the development of explainability methods for natural images, research specifically tailored for document images has been relatively scarce [41,40]. Moreover, in a recent benchmark study, Saifullah *et al.* [41] demonstrated that applying existing attribution-based XAI methods, commonly used in the natural image domain, to the document images presents several challenges, such as extensive noise in the output attributions, difficulty in interpreting explanations, and significant variation in explanations generated by different methods. In addition, the binary nature of document images poses a challenge in assessing whether a model emphasizes textual information in the foreground or comprehends the overall structural information of the document to arrive at its decision.

In this paper, we attempt to tackle the aforementioned challenges and propose a novel algorithm for generating explanations that takes into account the binary nature of the document images. Our approach mainly draws inspiration from the model-agnostic perturbation-based approaches [59,37,29], which assign importance to different image features by perturbing those features and evalu-

ating the perturbations’ impact on the model’s decision. However, it has been demonstrated that standard perturbation-based approaches [59,37,29] behave poorly when applied directly to document images [41], mainly due to the indiscriminate perturbation of image patches without regard for the structure in the data. To address this, we present an approach to independently segment the foreground and background features of the documents into different structural elements and at different levels of granularity, regardless of the document type. Then, feature ablation is applied to the segmented regions to allocate per-pixel importance, resulting in an image attribution map. Overall, the contributions of this paper can be summarized as follows:

- We introduce DocXplain, a model-agnostic explanation framework especially designed to generate fine-grained attribution maps for the task of document image classification. To the best of the authors’ knowledge, this is the first model-agnostic explanation framework specifically tailored for document images.
- We evaluate our proposed framework on the task of document image classification with 4 different evaluation metrics, 2 document datasets, and 10 distinct deep learning (DL) models, and compare the results with 9 existing state-of-the-art attribution methods. Through an exhaustive quantitative and qualitative analysis, we demonstrate that our approach either outperforms or performs comparably to existing state-of-the-art attribution-based approaches.

## 2 Related Work

### 2.1 eXplainable AI (XAI)

The field of XAI has been extensively explored in the past decade [7,36], resulting in a wide variety of approaches [49,48,52,29,37] for generating explanations regarding the predictions of black-box neural networks. In the following sections, we present a brief overview of the existing XAI methods.

**Feature attribution methods.** Feature attribution methods assign importance to input features or feature groups by locally estimating their relevance to the model’s decision, and they are particularly recognized for their post-hoc applicability. These methods can be broadly divided into two main categories: gradient-based approaches and perturbation-based approaches. Gradient-based methods such as Saliency [49], GradCAM [44], DeepLIFT [47], and IntegratedGradients [52] utilize gradient back-propagation inherent to black-box neural networks and assign importance to input features by approximating their contribution to the model gradients. In contrast, perturbation-based approaches, such as Occlusion [59] and Local Interpretable Model-Agnostic Explanations (LIME) [37], generate importance maps by perturbing the input features and evaluating the impact of perturbation on the model’s prediction, either directly or by estimating it through surrogate machine learning models.

SHapley Additive exPlanations (SHAP) is another popular group of feature-attribution approaches [29] that utilizes Shapley values—a game theory concept—to model feature importance. In this framework, each input feature is akin to a

*player* in a game, and the output of the model is treated as the *payout*, which corresponds to the importance of the input features. SHAP [29] has several extensions, each tailored to explain different types of machine learning models. For instance, TreeSHAP [28] is designed to explain the outputs of random forests through Shapley values. KernelSHAP [29] is a model-agnostic explanation framework that extends LIME [37] and computes Shapley values by training surrogate models on perturbed inputs. Similarly, DeepSHAP [29] extends the gradient-based approach of DeepLIFT [47] and utilizes the gradients of the model to generate the Shapley values for assigning feature importance.

**Concept-based approaches.** Concept-based approaches utilize predefined human-interpretable concepts to provide global explanations for machine learning models. The most prominent approach in this domain is Testing with Concept Activation Vectors (TCAV) [21] that utilizes concepts, such as stripes and textures in the case of natural images, to determine whether a neural network has learned relevant features from the data.

**Generative approaches.** Generative approaches have also gained considerable attention in recent years, notably due to their ability to generate high-quality and intuitive counterfactual explanations [23,20]. These approaches typically employ external generative models, such as generative adversarial networks (GANs) [11] or diffusion models [15], to synthesize features based on their relevance to the model’s prediction.

## 2.2 XAI in Document Image Analysis

While a plethora of research has gone into developing XAI methods for natural images, there has been relatively little exploration of XAI in the domain of document image analysis. The earliest work in this direction was conducted by Tensmeyer *et al.* (2017) [55], who investigated the intermediate layer activation maps to explain the decision-making of DL-powered document image classification models. Brini *et al.* [4] recently presented an end-to-end explanation framework for document layout analysis. Their approach, however, simply re-uses existing gradient-based methods [44,47] to generate the explanations for pre-annotated segmented regions. Saifullah *et al.* [41] presented an extensive benchmark of several existing state-of-the-art feature-attribution methods for the task of document image classification. In this work, they raised several concerns regarding the interpretability and fidelity of existing methods when applied to the document domain, noting that only a few techniques yielded sufficiently viable results. In another recent work, Saifullah *et al.* [40] presented DocXClassifier, an inherently interpretable document image classification model that combines a convolutional neural network (CNN) with attention-based pooling mechanism to produce attribution maps at inference. However, this method has some limitations of its own: (1) the model is only capable of generating coarse attribution maps, unable to highlight fine-grained features in the image, and (2) the approach is not model-agnostic, requiring modifications to existing neural network architectures and additional training.

### 3 DocXplain: Proposed Approach

In this section, we present our proposed explanation framework for generating fine-grained attribution maps for the task of document image classification. As illustrated in Fig. 1, our approach mainly comprises two stages: (1) Feature Segmentation and (2) Feature Ablation, both of which will be explained in detail in the following sections.

#### 3.1 Feature Segmentation

The first step in our approach involves segmenting the images into distinct features. Since we are dealing with document images, the features in this case correspond to both the black pixels representing the textual, tabular, or imagery content in the foreground and the white pixels representing the background. Note that various existing methods, including DL-based segmentation or optical-character-recognition (OCR) models, could have been utilized for segmenting the document images into relevant regions. However, while investigating these approaches, we noted that they are generally data-driven and capable of handling only specific types of inputs. For instance, an OCR model may perform poorly on handwritten text, making it unsuitable for generating reasonable segmentation maps for handwritten text documents. Therefore, to devise a more generic segmentation approach applicable to many different types of input documents, we opted to build it upon traditional image processing techniques. Formally, let  $I \in \mathbb{R}^{C \times H \times W}$  denote a full-page input document image. Then, our feature segmentation approach involves the following steps:

**Preprocessing.** The first step in our approach involves converting the image into a single-channel binary image ( $I \in \mathbb{R}^{H \times W}$ ) with black (foreground) and white (background) pixels. This can be easily achieved using standard image processing algorithms such as Otsu binarization [32]. It is important to note that here we assume sufficiently clean input document images (gray-scale or RGB) that can be effectively binarized into distinct background and foreground regions, which is a common scenario with business documents. In the second step of our approach, we downscale the images to a fixed resolution of  $1024 \times 1024$  without interpolation (to maintain the image in binary format) and apply the standard opening operation (dilation followed by erosion) with a  $5 \times 5$  filter to remove noise from the image.

**Background Segmentation.** While the foreground features, characterized by black pixels, are generally distinguishable in document images, the background simply consists of white pixels with no internal structure. Therefore, to segment the background, we generate a grid over the image with a fixed patch size of  $P_{bx} \times P_{by}$ . This results in the background segmentation matrix  $M_{bg} : \mathbb{X} \rightarrow \{1, \dots, n_{bg}\}$ ,  $\mathbb{X} = \{1, \dots, H\} \times \{1, \dots, W\}$  with a total of  $n_{bg} = \frac{W}{P_{bx}} \cdot \frac{H}{P_{by}}$  segmented regions over the whole image  $I \in \mathbb{R}^{H \times W}$ .

**Foreground Segmentation.** To segment the foreground regions, we first apply the standard dilation operation with a fixed kernel size of  $k \times k$  on the inverted image in order to consolidate foreground (text or imagery) regions into

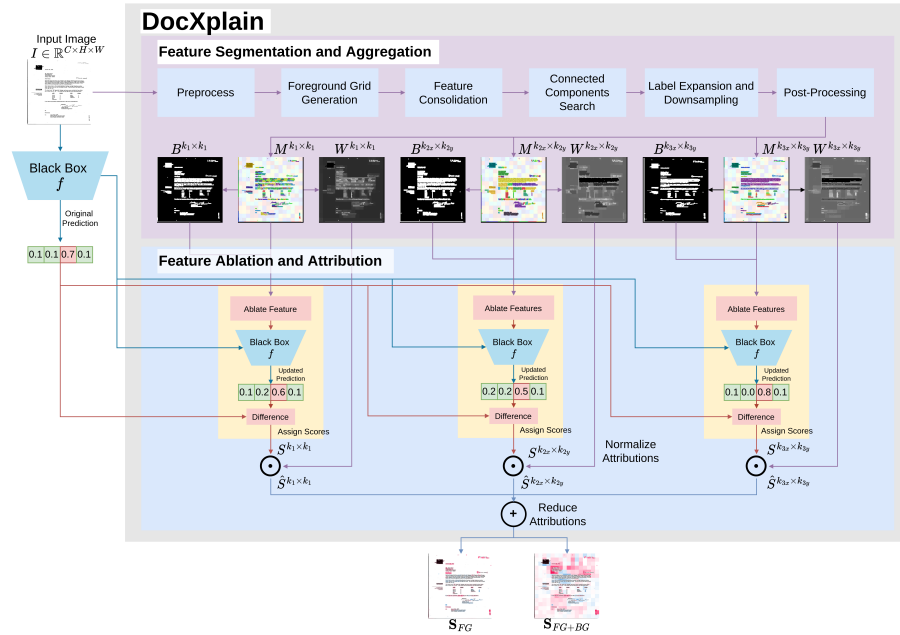


Fig. 1: An overview of the proposed approach, DocXplain, is presented. As shown, the image first undergoes several processing steps for generating segmentation maps at different kernel sizes. Then, given any black-box neural network  $f$ , per-kernel feature importance maps are generated by applying feature ablation in combination with the respective segmentation maps. Subsequently, the maps are summed to simultaneously create decoupled attribution maps for both background and foreground regions.  $\mathbf{S}_{FG}$  and  $\mathbf{S}_{FG+BG}$  correspond to the DocXplain<sub>FG</sub> DocXplain<sub>FG+BG</sub> settings, respectively.

blobs. Then, we apply connected components search on the image to assign a distinct label to each foreground blob, whereas all the white background pixels are assigned a fixed label of 0 at this stage. This yields a segmentation mask  $M_{fg} : \mathbb{X} \rightarrow \{0, \dots, n_{fg}\}$ , where  $n_{fg}$  represents the total number of foreground features extracted from the image. Note that depending on the specific requirements, different kernel sizes  $k_1 \times k_2$  may be used at this stage to obtain feature segmentation at different resolutions. Finally, we combine the two segmentation masks  $M_{bg}$  and  $M_{fg}$  by taking the following steps. We first offset the unique labels of  $M_{fg}$  by  $n_{bg}$  to generate a new foreground mask with the labels in the range  $\{0, 1 + n_{bg}, \dots, n_{fg} + n_{bg}\}$ . Notice that the offset is applied only to the foreground labels in  $M_{fg}$ , while the background label 0 remains unchanged. The combined segmentation mask  $M : \mathbb{X} \rightarrow \{1, \dots, n_{bg} + n_{fg}\}$  is then computed as follows:

$$M(\lambda \in \mathbb{X}) = \begin{cases} M_{bg}(\lambda) & \text{if } M_{fg}(\lambda) = 0 \text{ (background labels)} \\ M_{fg}(\lambda), & \text{else (foreground labels)} \end{cases} \quad (1)$$



Fig. 2: Segmentation maps generated by our approach for the kernels  $k_1 \times k_1 = 5 \times 5$ ,  $k_{2x} \times k_{2y} = 3 \times 15$ , and  $k_{3x} \times k_{3y} = 15 \times 3$  on a few randomly selected samples from the Tobacco3482 document dataset.

**Post Processing.** After generating the initial segmentation map, we perform label expansion on the foreground elements (where  $l > n_{bg}$ ) for  $N_{expansion}$  pixels and then downsample the image to a resolution required at the model input, such as  $224 \times 224$ , which is commonly utilized for deep-learning models. Label expansion at this step was necessary, as otherwise, downsampling an image to very small resolutions can result in the loss of important information about segmentation boundaries. For preprocessed images of resolution  $1024 \times 1024$ , we found that expanding the labels by 2 pixels ( $N_{expansion} = 2$ ) was suitable. In addition, downsampling was necessary at this stage to reduce the computational overhead for further processing. Despite these adjustments, two major issues remained:

1. There may be connected components left that span the entire image while occupying a very small area, such as tables or graphs. On the other hand, large figures or images may be represented as a single connected component while containing specific distinct features within.
2. The segmentation process may result in an extensively large number of small-sized noisy connected features, which can be computationally infeasible to process in later stages.

To address the first problem concerning large components such as tables, images, or figures, we utilize the Simple Linear Iterative Clustering (SLIC) [1] algorithm to further cluster these components into SLIC superpixels. As for the second problem, we mitigate it by performing a second stage of denoising, in which we substitute the labels of features with areas smaller than a fixed threshold with the corresponding background labels.

**Choice of Segmentation Kernels.** Since document images are semi-structured, it is challenging to assess whether, for a model’s prediction, an individual word, a text line, or a text block, and so forth, was found relevant. Therefore, in this work, we use 3 different sizes of kernels to segment the images at 3 different levels of granularity:

- A kernel of small size  $k_1 \times k_1$ , to generate segmentation maps for each individual textual content in the image.
- A kernel of size  $k_{2x} \times k_{2y}$ , such that  $k_{2y} \gg k_{2x}$ , to consolidate regions that are vertically close in distance, such as individual text blocks or a single column in tabular data.
- A kernel of size  $k_{3x} \times k_{3y}$ , where  $k_{3x} \gg k_{3y}$ , to consolidate regions that are horizontally aligned such as text lines.

Note that these kernel sizes can be considered hyperparameters and were chosen empirically for the datasets under consideration. In our experiments, we found that the configuration  $k_1 \times k_1 = 5 \times 5$ ,  $k_{2x} \times k_{2y} = 3 \times 15$ , and  $k_{3x} \times k_{3y} = 15 \times 3$ , worked the best. Fig. 2 illustrates the segmentation maps resulting from our approach using these three kernel sizes on a few randomly selected samples from the Tobacco3482 document dataset.

### 3.2 Feature Ablation

Let  $f : \mathcal{I} \rightarrow \mathbb{R}$  denote a black-box deep neural network to be explained, that for a given input image from the  $\mathcal{I} = \{I \mid I : \mathbb{X} \rightarrow R^C\}$ ,  $\mathbb{X} = \{1, \dots, H\} \times \{1, \dots, W\}$  with size  $H \times W$  and number of channels  $C$ , produces a scalar output confidence score. For the task of document image classification, the output of  $f$  is typically the prediction probability score for a given document class. Then, given the segmentation mask  $M : \mathbb{X} \rightarrow \{1, \dots, n_{bg} + n_{fg}\}$ , we define the importance of each feature group  $M_i = \{\lambda \in \mathbb{X} \mid M(\lambda) = i\}$ ,  $i \in \{1, \dots, n_{bg} + n_{fg}\}$  as the difference in confidence score observed when that feature is removed from the image  $I$ :

$$S_i = f(I) - f(I \setminus M_i) \quad (2)$$

where the term  $f(I \setminus M_i)$  represents the removal of feature  $M_i$  from the image  $I$ . Since document images are generally processed in gray-scale or binary format, we perform feature removal by substituting the pixel values of each foreground element with the background pixels and vice versa. More formally, for an image with pixel values normalized between 0 and 1, we use the following baseline matrix  $B : \mathbb{X} \rightarrow \{0, 1\}^C$  to replace the pixels of each feature group  $M_i$ :

$$B(\lambda \in \mathbb{X}) = \begin{cases} 0 & \text{if } M(\lambda) \leq n_{bg} \text{ (background regions)} \\ 1, & \text{else (foreground regions)} \end{cases} \quad (3)$$

Applying Eq. 2 on the model for all feature groups  $i \in \{1, \dots, n_{bg} + n_{fg}\}$  results in the output attribution score matrix  $S : \mathbb{X} \rightarrow \mathbb{R}$ , where  $S(\lambda \in \mathbb{X}) = \{S_i \mid M(\lambda) = i\}$ ,  $i \in \{1, \dots, n_{bg} + n_{fg}\}$ . Note that at this stage, since the attribution scores  $S$  are computed by removing grouped features in each iteration, the resulting scores are unnormalized with respect to the group size. For instance, removing larger feature groups will inherently result in larger drops in the model confidence as compared to the removal of smaller groups. To account for this bias, we normalize the attribution score of each feature set  $M_i$  by the inverse of the area occupied by it, and compute the final attribution score matrix as follows:

$$\hat{S} = S \odot \mathcal{W} \quad (4)$$



where  $\mathcal{W} : \mathbb{X} \rightarrow \mathbb{R}$  is the weight matrix defined as  $\mathcal{W}(\lambda \in \mathbb{X}) = \frac{1}{|\{\lambda \in \mathbb{X} | M(\lambda)=i\}|} = \frac{1}{|M_i|}$ ,  $i \in \{1, \dots, n_{bg} + n_{fg}\}$  and  $\odot$  denotes the element-wise multiplication. Finally, with  $K$  different segmentation masks  $M^k$ ,  $k \in \{1, \dots, K\}$ , the final attribution matrix  $\mathbf{S} : \mathbb{X} \rightarrow \mathbb{R}$  over each image can be simply computed as the sum of the normalized score matrices  $\hat{S}^k$  of each mask  $M^k$ :

$$\mathbf{S} = \sum_k^K \hat{S}^k \quad (5)$$

With our choice of kernels to generate 3 different segmentation maps, Eq. 5 can be rewritten as follows:

$$\mathbf{S} = \hat{S}^{k_1 \times k_1} + \hat{S}^{k_{2x} \times k_{2y}} + \hat{S}^{k_{3x} \times k_{3y}} \quad (6)$$

In all our experiments, we evaluate our approach under two settings: DocXplain<sub>FG</sub> and DocXplain<sub>FG+BG</sub>. In DocXplain<sub>FG</sub>, only the foreground segmented features are ablated, whereas, in DocXplain<sub>FG+BG</sub>, both foreground and background features are ablated, as illustrated in Fig. 1.

## 4 Experiment Setup

### 4.1 Datasets

We thoroughly investigate the effectiveness of our approach on two of the most widely used document image classification benchmarks: RVL-CDIP [12] and Tobacco3482<sup>4</sup>. RVL-CDIP [12] is a large-scale document image dataset with 16 equally distributed document classes and has been widely utilized as a benchmark for the task of document image classification [3, 2, 12, 8, 40, 19, 34]. The dataset showcases significant sample diversity, consisting of a total of 400,000 annotated document images with training, testing, and validation splits of sizes, 320,000, 40,000 and 40,000, respectively. The Tobacco3482<sup>1</sup> dataset, on the other hand, is small-scale, with only 3482 document samples divided into 10 different document types. In contrast to RVL-CDIP [12], however, this dataset has a significant class imbalance. In our experiments, we split this dataset into training, testing, and validation sets of sizes 2,504, 700, and 279, respectively.

### 4.2 Models

To evaluate the generalizability of our proposed approach across different model architectures, we choose 10 different deep learning models, namely, AlexNet [22], ResNet-50 [13], InceptionV3 [53], VGG-16 [25], MobileNetV3 [17], NFNet-F1 [5], DenseNet-121 [18], Res2Net-50[9], EfficientNet-B4 [54], and ConvNeXt-B [26]. Note that the same set of models was also previously investigated in the benchmark study by Saifullah *et al.* [41] and therefore provides a good comparison with the previous work. To train the models on the aforementioned datasets, we initialized them with ImageNet pretraining weights, first fine-tuned them on the

<sup>4</sup> <https://www.kaggle.com/datasets/patrickaudriaz/tobacco3482jpg>

Table 1: The performance of each model on the test sets of RVL-CDIP [12] and Tobacco3482 is listed. All the models were trained to achieve sufficiently high performance on the respective datasets for valid explainability analysis.

Datasets	Models									
	AlexNet	ResNet50	InceptionV3	VGG-16	MobileNetV3	NFNet-F1	DenseNet121	Res2Net50	EfficientNet-B4	ConvNeXt
RVL-CDIP (Acc %)	87.86	90.40	91.18	90.96	87.56	88.83	89.46	88.96	92.68	<b>93.89</b>
Tobacco3482 (Acc %)	88.85	92.00	92.71	93.71	85.85	91.28	92.14	89.85	93.85	<b>94.71</b>

RVL-CDIP [12] dataset, and then further fine-tuned them on the Tobacco3482 dataset. In particular, the first 8 models were trained using the approach proposed by Afzal *et al.* (2017) [2], whereas the remaining two models, EfficientNet-B4 [54] and ConvNeXt-B [26], were trained using the methodologies outlined in the original works by Ferrando *et al.* [8] and Saifullah *et al.* [40], respectively, in which these models were proposed for the task of document image classification. Following previous works [2,8,40], for all models, except EfficientNet-B4 and ConvNeXt-B, we utilized input image resolutions of  $224 \times 224$ , while for these two models, we used input image resolutions of  $384 \times 384$ . The performance achieved by the models on the respective test sets is given in Table. 1.

### 4.3 XAI Methods

We compare our approach with 9 different existing attribution-based methods, which include Saliency [49], GuidedBackprop [51], IntegratedGradients [52], InputXGradient [48], and DeepLIFT [47], SHAP-based methods including DeepSHAP [29] and KernelSHAP [29], and perturbation-based methods including LIME [37] and Occlusion [59]. For all the gradient-based methods, we use default parameters for computing attributions. For segmentation-based perturbation-based approaches KernelSHAP [29] and LIME [37], we directly apply the SLIC [1] algorithm to generate superpixels as proposed in LIME [37] and then train the surrogate models. For DeepSHAP [29], we utilize a background distribution of 100 samples for each sample, which we found sufficient for computing the attributions. Note that increasing the number of samples in this background distribution may enhance performance, but it also leads to extensively high computational requirements, which we found infeasible for our experiments. Finally, we apply Occlusion [59] with a patch size of  $16 \times 16$  and a stride of  $8 \times 8$  for images of size  $224 \times 224$  and a patch size of  $32 \times 32$  and a stride of  $16 \times 16$  for images of size  $384 \times 384$ . Again, it is worth mentioning that decreasing the patch size in Occlusion [59] may result in more fine-grained attributions but at huge computational costs.

### 4.4 Evaluation Metrics

We perform a quantitative comparison of our approach with existing state-of-the-art explainability methods using 4 well-established evaluation metrics: Area Over the Perturbation Curve (AOPC) [43], Sensitivity [58], Infidelity [58], and Continuity [42].

**AOPC** [43] measures the faithfulness of attributions by removing patches of the most relevant and least relevant image regions and subsequently computing

the area over the model’s confidence curve for a given target class. In this work,  $\text{AOPC}_{\text{MoRF}}$  corresponds to the AOPC curves generated by removing the top most relevant features from the image, while  $\text{AOPC}_{\text{LeRF}}$  corresponds to removing the least most relevant features. Higher values of  $\text{AOPC}_{\text{MoRF}}$  and lower values of  $\text{AOPC}_{\text{LeRF}}$  correspond to more faithful explanations. Another metric is the **Area Between the Perturbation Curves (ABPC)** [43], which summarizes the AOPC metric into a scalar value as the area between the  $\text{AOPC}_{\text{MoRF}}$  and the  $\text{AOPC}_{\text{LeRF}}$  curves. Larger ABPC values correspond to better explanations. In this work, we compute the AOPC metrics by removing patches of size  $8 \times 8$  from the input samples using a pixel-flipping scheme where the white background regions are flipped to black and vice versa.

**Sensitivity** [58] and **Infidelity** [58] both gauge the faithfulness and fidelity of explanations under input perturbations, with smaller values corresponding to better explanations for both of these metrics.

**Continuity** [42] is useful for measuring the overall interpretability of the attribution maps. It is computed by taking the mean of absolute gradients of the attribution map across horizontal and vertical directions. Smaller values for Continuity are desirable for better interpretability.

To evaluate the metrics on the RVL-CDIP [12] dataset, we utilized 4000 randomly sampled images from the test set for all models, except EfficientNet-B4 [54] and ConvNeXt-B [26]. For these two models, we limited the evaluation to 1000 test samples due to their extremely high computational requirements. For the Tobacco3482 dataset, we computed all metrics on the entire test set consisting of 700 image samples. In all experiments carried out in this work, we evaluate the attribution maps generated for the correctly predicted class.

## 5 Experiment Results

In this section, we begin with a qualitative assessment of our proposed approach in comparison to existing attribution methods. Subsequently, we present the results of the quantitative evaluation of our approach using different evaluation metrics discussed in Section 4.4.

### 5.1 Qualitative Comparison

In Fig. 3, we compare the explanations generated for the ConvNeXt-B [26] model by our proposed approach under two different settings,  $\text{DocXplain}_{\text{FG+BG}}$  and  $\text{DocXplain}_{\text{FG}}$ , with those generated by 5 existing attribution methods on 6 randomly selected samples from the RVL-CDIP [12] dataset. Several notable observations can be drawn from these results. Firstly, it is directly evident from the quality of attributions that both gradient-based approaches (Saliency [49], and DeepLIFT [47]) and perturbation-based approaches (KernelSHAP [29]) perform significantly poorer compared to our proposed approach, especially under the  $\text{DocXplain}_{\text{FG}}$  setting. On the other hand, Occlusion [59] exhibited noticeable similarities with our approach. Particularly, it can be observed that our approach generates structurally similar attribution maps to Occlusion [59] when applied under the  $\text{DocXplain}_{\text{FG+BG}}$ , suggesting a consensus between our approach and

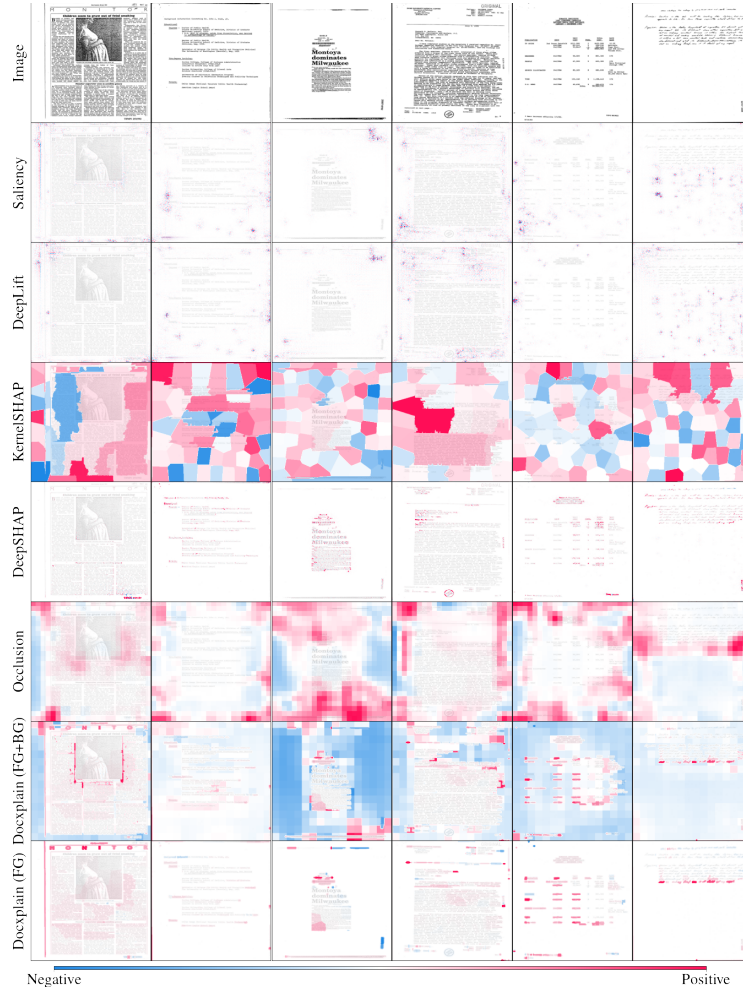


Fig. 3: Explanations generated by different attribution methods for the ConvNeXt-B [26] model on 6 randomly selected samples from the RVL-CDIP dataset. As evident, our approach under both settings (DocXplain<sub>FG</sub> and DocXplain<sub>FG+BG</sub>) produces significantly fine-grained attribution maps compared to existing methods. In addition, examining the two settings in combination allows decoupling whether an entire region or only specific foreground regions in the image are considered important by the model, significantly improving the interpretability of attributions.

Occlusion [59] on the importance of regions in the image. However, it is also noticeable that, compared to Occlusion [59], our approach produces significantly more interpretable maps, with concrete regions of importance, owing to the distinct boundaries between the foreground and background regions. Furthermore, examining the attribution maps of both DocXplain<sub>FG</sub> and DocXplain<sub>FG+BG</sub> in

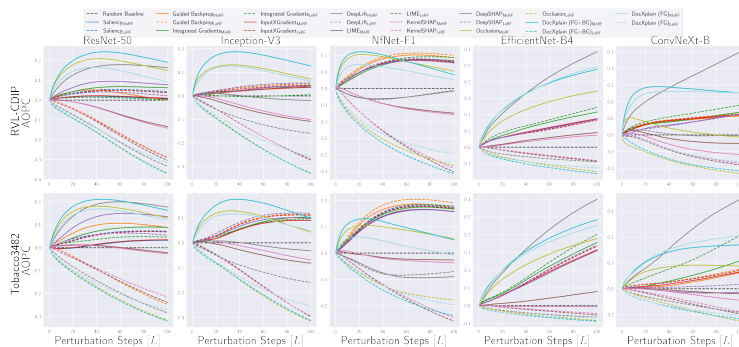


Fig. 4: A comparison of  $\text{AOPC}_{\text{MoRF}}$  and  $\text{AOPC}_{\text{LeRF}}$  of different methods, plotted relative to the random baseline, across 5 selected deep neural networks. As evident from the steep rise and steep descent in the  $\text{AOPC}_{\text{MoRF}}$  and  $\text{AOPC}_{\text{LeRF}}$  curves of our approach under both settings, it demonstrates significantly high faithfulness compared to other methods.

combination allows distinguishing whether an entire region is important (including both foreground and background) or only a specific textual or image foreground feature in a given region holds significance. In contrast, when comparing DeepSHAP [29] with the DocXplain<sub>FG</sub> setting, although the two approaches showed a slight visual resemblance, they diverged significantly on the importance of features. While in some cases, they reached a consensus, in others they exhibited major discrepancies with opposite attributions assigned to some features. In addition, it can be observed that DeepSHAP [29] generally produced highly sparse attribution maps, sometimes only lightly highlighting the boundaries of text strokes or individual letters. In contrast, our approach under the DocXplain<sub>FG</sub> setting assigns importance to complete words, textual lines, text blocks, and structural elements such as images and tables in the image, allowing for significantly better interpretability. Additional qualitative results across different models and methods are presented in Appendix A.

## 5.2 Quantitative Comparison

In Fig. 4, we compare the AOPCs of our proposed method (under both DocXplain<sub>FG</sub> and DocXplain<sub>FG+BG</sub> settings) with existing attribution approaches on 5 different deep neural networks investigated in this work. Firstly, it can be observed that in terms of the AOPCs, our proposed approach demonstrated the best faithfulness across various models on both datasets, RVL-CDIP [12] and Tobacco3482. This is evident from the steep rise and steep descent in the  $\text{AOPC}_{\text{MoRF}}$  and  $\text{AOPC}_{\text{LeRF}}$  curves of our approach, respectively, in comparison to the other methods. Another noteworthy observation is that, even under the DocXplain<sub>FG</sub> setting, where we only utilize the foreground features for generating explanations, our approach demonstrated significantly better faithfulness compared to other methods. In some cases, it performed similarly to Occlusion [59], as observed in the case of ResNet-50 [13] and InceptionV3 [53] models, while in other

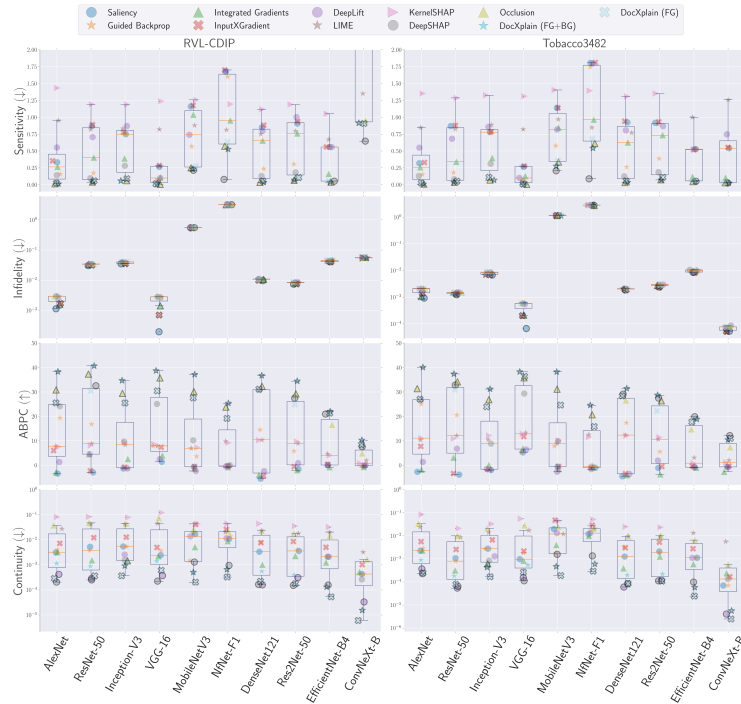


Fig. 5: The results of 4 metrics, Sensitivity [58], Infidelity [58], Continuity [42], and ABPC [43] obtained by each method for each model on the X-axis. It can be observed that our approach, under both settings, either outperforms or performs comparably to existing state-of-the-art attribution-based approaches on various explainability metrics.

cases, such as ConvNeX-B [26] and EfficientNet-B4 [54], it performed on a similar scale to DocXplain<sub>FG+BG</sub> setting. Furthermore, comparing the AOPCs of the two settings, DocXplain<sub>FG+BG</sub> and DocXplain<sub>FG</sub>, provides valuable insight into whether a given model prioritizes only the foreground regions or focuses on both foreground and background for making a decision. Notably, for both ConvNeX-B [26] and EfficientNet-B4 [54], the AOPC<sub>MoRF</sub> curves for DocXplain<sub>FG</sub> and DocXplain<sub>FG+BG</sub> closely align, indicating that these models assign relatively little importance to the background features in comparison to the other models. For additional comparison of AOPC on other models, see Appendix. B.1.

In Fig. 5, we present a quantitative evaluation of our approach against existing explainability methods, in terms of the Sensitivity [58], Infidelity [58], Continuity [42], and the ABPC [43] metrics. In particular, for each model on the X-axis, we make a box plot that summarizes the overall distribution of the metrics across the explainability methods and additionally plot the raw metric values for each attribution method for direct comparison. First, directing our attention to the Sensitivity [58] metric, it can be observed that our pro-

posed approach under both settings performs equally well to the Occlusion [59] and DeepSHAP [29] approach, resulting in the lowest Sensitivity [58] across the majority of models. Interestingly, on the NFNet-F1 [5] model, DeepSHAP [29] scored considerably low on Sensitivity [58] compared to both Occlusion [59] and our proposed approach. However, upon closer inspection of the corresponding ABPC scores, it becomes evident that DeepSHAP [29], along with many gradient-based approaches, performed extremely poorly on the ABPC metric on this model, indicating highly unfaithful explanations. This observation aligns with the findings of the previous study [41], where DeepSHAP [29] experienced failures on certain models, resulting in extremely poor attribution maps. Additional support for this observation is provided through supplementary qualitative results in Appendix A.2.

Focusing on the Infidelity [58] metric, it can be observed that all the approaches exhibited comparable and consistently low infidelity scores with minimal variance between the methods. However, on VGG-16 [25] and AlexNet [22], the gradient-based approaches (especially Saliency [49]) appeared to perform slightly better on this metric. On the ABPC metric [43], which summarizes the results of the AOPC curves, we can observe that our approach greatly outperformed all existing approaches under the DocXplain<sub>FG+BG</sub> setting, whereas DocXplain<sub>FG</sub> performed comparably to DeepSHAP [29] and Occlusion [59], indicating better faithfulness. Finally, on the Continuity metric [42], which captures the interpretability of a method, our DocXplain<sub>FG</sub> approach consistently outperformed the majority of approaches and only occasionally fell behind DeepLIFT [47] and DeepSHAP [29]. On the other hand, DocXplain<sub>FG+BG</sub> lagged slightly behind the three methods (DeepLIFT [47], DeepSHAP [29], and DocXplain<sub>FG</sub>), indicating poorer interpretability in comparison. Note that this relatively poorer interpretability of DocXplain<sub>FG+BG</sub> is also evident from the qualitative results in Fig. 3, where, when observed independently of DocXplain<sub>FG</sub>, the interpretation of attribution maps was challenging. However, it is also worth noting that, despite the similarities in qualitative results with Occlusion [59], DocXplain<sub>FG+BG</sub> still resulted in significantly lower Continuity [42] scores than the latter (notice the log scale). For a more detailed examination, the raw metric values for all the attribution methods are also provided in Appendix B.2.

## 6 Conclusion

In this paper, we presented a novel model-agnostic explainability method especially designed for document image classification. Through a thorough qualitative and quantitative evaluation of our approach across different settings and various metrics, we demonstrated the superiority of our approach compared to existing methods in terms of both faithfulness and interpretability. In addition, we demonstrated how our approach enables decoupling the foreground and background feature importance, enhancing the interpretation of attribution maps. Future efforts could focus on refining the segmentation approach by combining it with optical-character-recognition (OCR) models for direct text localization. In addition, it could be worthwhile to explore extending this approach to other document image analysis tasks and to multimodal document analysis models.

## References

1. Achanta, R., Shaji, A., Smith, K., Lucchi, A., Fua, P., Süsstrunk, S.: Slic superpixels compared to state-of-the-art superpixel methods. *IEEE Transactions on Pattern Analysis and Machine Intelligence* **34**(11), 2274–2282 (2012). <https://doi.org/10.1109/TPAMI.2012.120>
2. Afzal, M., Kolsch, A., Ahmed, S., Liwicki, M.: Cutting the error by half: Investigation of very deep cnn and advanced training strategies for document image classification. In: 2017 14th IAPR International Conference on Document Analysis and Recognition (ICDAR). pp. 883–888. IEEE Computer Society, Los Alamitos, CA, USA (nov 2017). <https://doi.org/10.1109/ICDAR.2017.149>, <https://doi.ieeecomputersociety.org/10.1109/ICDAR.2017.149>
3. Afzal, M.Z., Capobianco, S., Malik, M.I., Marinai, S., Breuel, T.M., Dengel, A., Liwicki, M.: Deepdocclassifier: Document classification with deep convolutional neural network. In: 2015 13th International Conference on Document Analysis and Recognition (ICDAR). pp. 1111–1115 (2015). <https://doi.org/10.1109/ICDAR.2015.7333933>
4. Brini, I., Mehri, M., Ingold, R., Essoukri Ben Amara, N.: An end-to-end framework for evaluating explainable deep models: Application to historical document image segmentation. In: Nguyen, N.T., Manolopoulos, Y., Chbeir, R., Kozierekiewicz, A., Trawiński, B. (eds.) *Computational Collective Intelligence*. pp. 106–119. Springer International Publishing, Cham (2022)
5. Brock, A., De, S., Smith, S.L., Simonyan, K.: High-performance large-scale image recognition without normalization. In: Meila, M., Zhang, T. (eds.) *Proceedings of the 38th International Conference on Machine Learning*. *Proceedings of Machine Learning Research*, vol. 139, pp. 1059–1071. PMLR (18–24 Jul 2021), <https://proceedings.mlr.press/v139/brock21a.html>
6. Carlini, N., Wagner, D.: Towards evaluating the robustness of neural networks. In: 2017 IEEE Symposium on Security and Privacy (SP). pp. 39–57. IEEE Computer Society, Los Alamitos, CA, USA (may 2017). <https://doi.org/10.1109/SP.2017.49>, <https://doi.ieeecomputersociety.org/10.1109/SP.2017.49>
7. Carvalho, D.V., Pereira, E.M., Cardoso, J.S.: Machine learning interpretability: A survey on methods and metrics. *Electronics* **8**(8) (2019). <https://doi.org/10.3390/electronics8080832>, <https://www.mdpi.com/2079-9292/8/8/832>
8. Ferrando, J., Domínguez, J.L., Torres, J., García, R., García, D., Garrido, D., Cortada, J., Valero, M.: Improving accuracy and speeding up document image classification through parallel systems. In: Krzhizhanovskaya, V.V., Závodszy, G., Lees, M.H., Dongarra, J.J., Sloot, P.M.A., Brissos, S., Teixeira, J. (eds.) *Computational Science – ICCS 2020*. pp. 387–400. Springer International Publishing, Cham (2020)
9. Gao, S.H., Cheng, M.M., Zhao, K., Zhang, X.Y., Yang, M.H., Torr, P.: Res2net: A new multi-scale backbone architecture. *IEEE Transactions on Pattern Analysis and Machine Intelligence* **43**(2), 652–662 (feb 2021). <https://doi.org/10.1109/tpami.2019.2938758>, <https://doi.org/10.1109%2Ftpami.2019.2938758>
10. Geirhos, R., Rubisch, P., Michaelis, C., Bethge, M., Wichmann, F.A., Brendel, W.: Imagenet-trained CNNs are biased towards texture; increasing shape bias improves accuracy and robustness. In: *International Conference on Learning Representations* (2019), <https://openreview.net/forum?id=Bygh9j09KX>
11. Goodfellow, I.J., Pouget-Abadie, J., Mirza, M., Xu, B., Warde-Farley, D., Ozair, S., Courville, A., Bengio, Y.: Generative Adversarial Networks (Jun 2014), <https://arxiv.org/abs/1406.2661>



12. Harley, A.W., Ufkes, A., Derpanis, K.G.: Evaluation of deep convolutional nets for document image classification and retrieval. In: 2015 13th International Conference on Document Analysis and Recognition (ICDAR). pp. 991–995 (2015). <https://doi.org/10.1109/ICDAR.2015.7333910>
13. He, K., Zhang, X., Ren, S., Sun, J.: Deep residual learning for image recognition. 2016 IEEE Conference on Computer Vision and Pattern Recognition (CVPR) pp. 770–778 (2016)
14. Hendrycks, D., Dietterich, T.: Benchmarking neural network robustness to common corruptions and perturbations. In: International Conference on Learning Representations (2019), <https://openreview.net/forum?id=HJz6tiCqYm>
15. Ho, J., Jain, A., Abbeel, P.: Denoising diffusion probabilistic models (2020). <https://doi.org/10.48550/ARXIV.2006.11239>, <https://arxiv.org/abs/2006.11239>
16. Hooker, S., Moorosi, N., Clark, G., Bengio, S., Denton, E.: Characterising bias in compressed models (2020)
17. Howard, A.G., Zhu, M., Chen, B., Kalenichenko, D., Wang, W., Weyand, T., Andreetto, M., Adam, H.: Mobilenets: Efficient convolutional neural networks for mobile vision applications (2017)
18. Huang, G., Liu, Z., van der Maaten, L., Weinberger, K.Q.: Densely connected convolutional networks. In: Proceedings of the IEEE Conference on Computer Vision and Pattern Recognition (CVPR) (July 2017)
19. Huang, Y., Lv, T., Cui, L., Lu, Y., Wei, F.: Layoutlmv3: Pre-training for document ai with unified text and image masking. In: Proceedings of the 30th ACM International Conference on Multimedia. p. 4083–4091. MM '22, Association for Computing Machinery, New York, NY, USA (2022). <https://doi.org/10.1145/3503161.3548112>, <https://doi.org/10.1145/3503161.3548112>
20. Jeanneret, G., Simon, L., Jurie, F.: Diffusion models for counterfactual explanations (2022)
21. Kim, B., Wattenberg, M., Gilmer, J., Cai, C.J., Wexler, J., Viégas, F.B., Sayres, R.: Interpretability beyond feature attribution: Quantitative testing with concept activation vectors (tcav). In: Dy, J.G., Krause, A. (eds.) ICML. Proceedings of Machine Learning Research, vol. 80, pp. 2673–2682. PMLR (2018), <http://dblp.uni-trier.de/db/conf/icml/icml2018.html#KimWGCWVS18>
22. Krizhevsky, A., Sutskever, I., Hinton, G.E.: Imagenet classification with deep convolutional neural networks. In: Proceedings of the 25th International Conference on Neural Information Processing Systems - Volume 1. p. 1097–1105. NIPS'12, Curran Associates Inc., Red Hook, NY, USA (2012)
23. Lang, O., Gandselman, Y., Yarom, M., Wald, Y., Elidan, G., Hassidim, A., Freeman, W.T., Isola, P., Globerson, A., Irani, M., Mosseri, I.: Explaining in style: Training a gan to explain a classifier in stylespace (2021)
24. Li, M., Xu, Y., Cui, L., Huang, S., Wei, F., Li, Z., Zhou, M.: DocBank: A benchmark dataset for document layout analysis. In: Scott, D., Bel, N., Zong, C. (eds.) Proceedings of the 28th International Conference on Computational Linguistics. pp. 949–960. International Committee on Computational Linguistics, Barcelona, Spain (Online) (Dec 2020). <https://doi.org/10.18653/v1/2020.coling-main.82>, <https://aclanthology.org/2020.coling-main.82>
25. Liu, S., Deng, W.: Very deep convolutional neural network based image classification using small training sample size. In: 2015 3rd IAPR Asian Conference on Pattern Recognition (ACPR). pp. 730–734 (2015). <https://doi.org/10.1109/ACPR.2015.7486599>

26. Liu, Z., Mao, H., Wu, C.Y., Feichtenhofer, C., Darrell, T., Xie, S.: A convnet for the 2020s. In: Proceedings of the IEEE/CVF Conference on Computer Vision and Pattern Recognition (CVPR). pp. 11976–11986 (June 2022)
27. Lucieri, A., Schmeisser, F., Balada, C.P., Siddiqui, S.A., Dengel, A., Ahmed, S.: Revisiting the shape-bias of deep learning for dermoscopic skin lesion classification. In: Yang, G., Aviles-Rivero, A., Roberts, M., Schönlieb, C.B. (eds.) Medical Image Understanding and Analysis. pp. 46–61. Springer International Publishing, Cham (2022)
28. Lundberg, S.M., Erion, G.G., Lee, S.I.: Consistent individualized feature attribution for tree ensembles (2019)
29. Lundberg, S.M., Lee, S.I.: A unified approach to interpreting model predictions. In: Proceedings of the 31st International Conference on Neural Information Processing Systems. p. 4768–4777. NIPS’17, Curran Associates Inc., Red Hook, NY, USA (2017)
30. Nemirovsky, D., Thiebaut, N., Xu, Y., Gupta, A.: CounterGAN: Generating counterfactuals for real-time recourse and interpretability using residual GANs. In: Cussens, J., Zhang, K. (eds.) Proceedings of the Thirty-Eighth Conference on Uncertainty in Artificial Intelligence. Proceedings of Machine Learning Research, vol. 180, pp. 1488–1497. PMLR (01–05 Aug 2022), <https://proceedings.mlr.press/v180/nemirovsky22a.html>
31. Ntoutsis, E., Fafalios, P., Gadiraju, U., Iosifidis, V., Nejdli, W., Vidal, M.E., Ruggieri, S., Turini, F., Papadopoulos, S., Krasanakis, E., Kompatsiaris, I., Kinder-Kurlanda, K., Wagner, C., Karimi, F., Fernandez, M., Alani, H., Berendt, B., Kruegel, T., Heinze, C., Broelemann, K., Kasneci, G., Tiropanis, T., Staab, S.: Bias in data-driven artificial intelligence systems—an introductory survey. WIREs Data Mining and Knowledge Discovery **10**(3), e1356 (2020). <https://doi.org/https://doi.org/10.1002/widm.1356>, <https://wires.onlinelibrary.wiley.com/doi/abs/10.1002/widm.1356>
32. Otsu, N.: A threshold selection method from gray level histograms. IEEE Transactions on Systems, Man, and Cybernetics **9**, 62–66 (1979)
33. Pfitzmann, B., Auer, C., Dolfi, M., Nassar, A.S., Staar, P.: Doclaynet: A large human-annotated dataset for document-layout segmentation. In: Proceedings of the 28th ACM SIGKDD Conference on Knowledge Discovery and Data Mining. KDD ’22, ACM (Aug 2022). <https://doi.org/10.1145/3534678.3539043>, <http://dx.doi.org/10.1145/3534678.3539043>
34. Powalski, R., Borchmann, Ł., Jurkiewicz, D., Dwojak, T., Pietruszka, M., Pałka, G.: Going full-tilt boogie on document understanding with text-image-layout transformer. In: Lladós, J., Lopresti, D., Uchida, S. (eds.) Document Analysis and Recognition – ICDAR 2021. pp. 732–747. Springer International Publishing, Cham (2021)
35. Project, T.A.: Shabbypages: A reproducible document denoising and binarization dataset (2023), <https://github.com/sparkfish/shabby-pages>
36. Ras, G., Xie, N., van Gerven, M., Doran, D.: Explainable deep learning: A field guide for the uninitiated. J. Artif. Int. Res. **73** (may 2022). <https://doi.org/10.1613/jair.1.13200>, <https://doi.org/10.1613/jair.1.13200>
37. Ribeiro, M., Singh, S., Guestrin, C.: “why should I trust you?”: Explaining the predictions of any classifier. In: DeNero, J., Finlayson, M., Reddy, S. (eds.) Proceedings of the 2016 Conference of the North American Chapter of the Association for Computational Linguistics: Demonstrations. pp. 97–101. Association for Computational Linguistics, San Diego, California (Jun 2016). <https://doi.org/10.18653/v1/N16-3020>, <https://aclanthology.org/N16-3020>

38. Rudin, C.: Stop explaining black box machine learning models for high stakes decisions and use interpretable models instead. *Nature machine intelligence* **1**(5), 206–215 (2019)
39. Saifullah, S., Siddiqui, S.A., Agne, S., Dengel, A., Ahmed, S.: Are deep models robust against real distortions? a case study on document image classification. In: 2022 26th International Conference on Pattern Recognition (ICPR). pp. 1628–1635 (2022). <https://doi.org/10.1109/ICPR56361.2022.9956167>
40. Saifullah, S., Agne, S., Dengel, A., Ahmed, S.: DocXClassifier: Towards a Robust and Interpretable Deep Neural Network for Document Image Classification (10 2023). <https://doi.org/10.36227/techrxiv.19310489.v5>, [https://www.techrxiv.org/articles/preprint/DocXClassifier\\_High\\_Performance\\_Explainable\\_Deep\\_Network\\_for\\_Document\\_Image\\_Classification/19310489](https://www.techrxiv.org/articles/preprint/DocXClassifier_High_Performance_Explainable_Deep_Network_for_Document_Image_Classification/19310489)
41. Saifullah, S., Agne, S., Dengel, A., Ahmed, S.: The reality of high performing deep learning models: A case study on document image classification (Oct 2023). <https://doi.org/10.36227/techrxiv.19310537.v3>, <http://dx.doi.org/10.36227/techrxiv.19310537.v3>
42. Saifullah, S., Mercier, D., Lucieri, A., Dengel, A., Ahmed, S.: Privacy meets explainability: A comprehensive impact benchmark (2022)
43. Samek, W., Binder, A., Montavon, G., Lapuschkin, S., Müller, K.R.: Evaluating the visualization of what a deep neural network has learned. *IEEE Transactions on Neural Networks and Learning Systems* **28**, 2660–2673 (11 2017). <https://doi.org/10.1109/TNNLS.2016.2599820>
44. Selvaraju, R.R., Cogswell, M., Das, A., Vedantam, R., Parikh, D., Batra, D.: Grad-cam: Visual explanations from deep networks via gradient-based localization. *International Journal of Computer Vision* **128**(2), 336–359 (Oct 2019). <https://doi.org/10.1007/s11263-019-01228-7>, <http://dx.doi.org/10.1007/s11263-019-01228-7>
45. Shen, Z., Zhang, R., Dell, M., Lee, B.C.G., Carlson, J., Li, W.: Layoutparser: A unified toolkit for deep learning based document image analysis (2021)
46. Shrestha, S., Das, S.: Exploring gender biases in ml and ai academic research through systematic literature review. *Frontiers in Artificial Intelligence* **5** (Oct 2022). <https://doi.org/10.3389/frai.2022.976838>, <http://dx.doi.org/10.3389/frai.2022.976838>
47. Shrikumar, A., Greenside, P., Kundaje, A.: Learning important features through propagating activation differences. In: Proceedings of the 34th International Conference on Machine Learning - Volume 70. p. 3145–3153. ICML'17, JMLR.org (2017)
48. Shrikumar, A., Greenside, P., Shcherbina, A., Kundaje, A.: Not just a black box: Learning important features through propagating activation differences (2017)
49. Simonyan, K., Vedaldi, A., Zisserman, A.: Deep inside convolutional networks: Visualising image classification models and saliency maps. *CoRR* **abs/1312.6034** (2013), <https://api.semanticscholar.org/CorpusID:1450294>
50. Smilkov, D., Thorat, N., Kim, B., Viégas, F.B., Wattenberg, M.: Smoothgrad: removing noise by adding noise. *ArXiv* **abs/1706.03825** (2017), <https://api.semanticscholar.org/CorpusID:11695878>
51. Springenberg, J., Dosovitskiy, A., Brox, T., Riedmiller, M.: Striving for simplicity: The all convolutional net. In: ICLR (workshop track) (2015), <http://lmb.informatik.uni-freiburg.de/Publications/2015/DB15a>
52. Sundararajan, M., Taly, A., Yan, Q.: Axiomatic attribution for deep networks. In: International conference on machine learning. pp. 3319–3328. PMLR (2017)

53. Szegedy, C., Vanhoucke, V., Ioffe, S., Shlens, J., Wojna, Z.: Rethinking the inception architecture for computer vision. In: 2016 IEEE Conference on Computer Vision and Pattern Recognition (CVPR). pp. 2818–2826. IEEE Computer Society, Los Alamitos, CA, USA (jun 2016). <https://doi.org/10.1109/CVPR.2016.308>, <https://doi.ieeecomputersociety.org/10.1109/CVPR.2016.308>
54. Tan, M., Le, Q.: EfficientNet: Rethinking model scaling for convolutional neural networks. In: Chaudhuri, K., Salakhutdinov, R. (eds.) Proceedings of the 36th International Conference on Machine Learning. Proceedings of Machine Learning Research, vol. 97, pp. 6105–6114. PMLR (09–15 Jun 2019), <https://proceedings.mlr.press/v97/tan19a.html>
55. Tensmeyer, C., Martinez, T.: Analysis of convolutional neural networks for document image classification. In: 2017 14th IAPR International Conference on Document Analysis and Recognition (ICDAR). vol. 01, pp. 388–393 (2017). <https://doi.org/10.1109/ICDAR.2017.71>
56. Varshney, K.R., Alemzadeh, H.: On the safety of machine learning: Cyber-physical systems, decision sciences, and data products. *Big Data* **5**(3), 246–255 (2017). <https://doi.org/10.1089/big.2016.0051>, <https://doi.org/10.1089/big.2016.0051>, PMID: 28933947
57. Wexler, R.: When a computer program keeps you in jail: How computers are harming criminal justice. <https://www.nytimes.com/2017/06/13/opinion/how-computers-are-harming-criminal-justice.html> (Jun 2017)
58. Yeh, C.K., Hsieh, C.Y., Suggala, A.S., Inouye, D.I., Ravikumar, P.: On the (in)fideliity and sensitivity of explanations. In: Wallach, H.M., Larochelle, H., Beygelzimer, A., d’Alché Buc, F., Fox, E.B., Garnett, R. (eds.) NeurIPS. pp. 10965–10976 (2019), <http://dblp.uni-trier.de/db/conf/nips/nips2019.html#YehHSIR19>
59. Zeiler, M.D., Fergus, R.: Visualizing and understanding convolutional networks. In: Fleet, D., Pajdla, T., Schiele, B., Tuytelaars, T. (eds.) Computer Vision – ECCV 2014. pp. 818–833. Springer International Publishing, Cham (2014)

## Appendix A Additional Qualitative Results

### A.1 Additional Qualitative Comparison of Methods

In Fig. 6, Fig. 7, and Fig. 8, we show additional results for the explanations generated by different explainability methods for the ConvNeXt-B [26], EfficientNet-B4 [54], and ResNet-50 [13] models, respectively, on 6 random selected images from the RVL-CDIP [12] dataset. By examining the figures across the models,

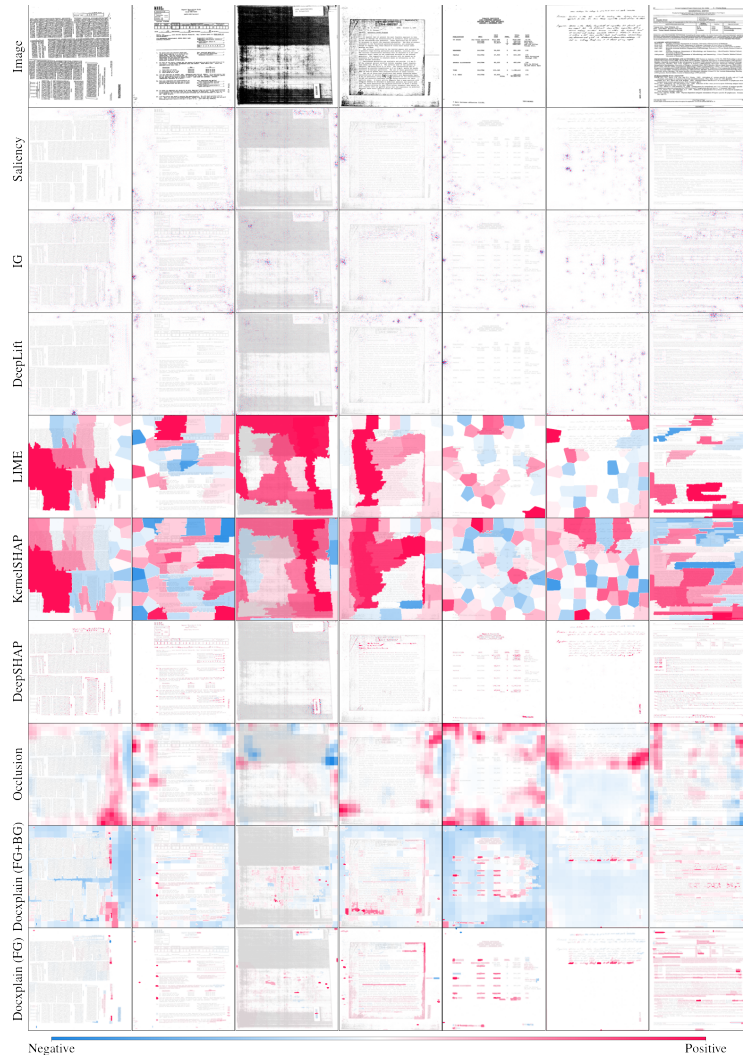


Fig. 6: Additional comparison of explanations generated for the ConvNeXt-B [26] model by different attribution methods on 7 randomly selected samples from the RVL-CDIP [12] dataset.

it can be noted that our observations from Section. 5.1 about the gradient-based approaches and perturbation-based approaches remain consistent across different models. Similarly, our observations regarding the similarities between Occlusion [59] and DocXplain<sub>FG+BG</sub>, as well as the diverging consensus between DocXplain<sub>FG</sub> and DeepSHAP [29], also remain consistent across different models.

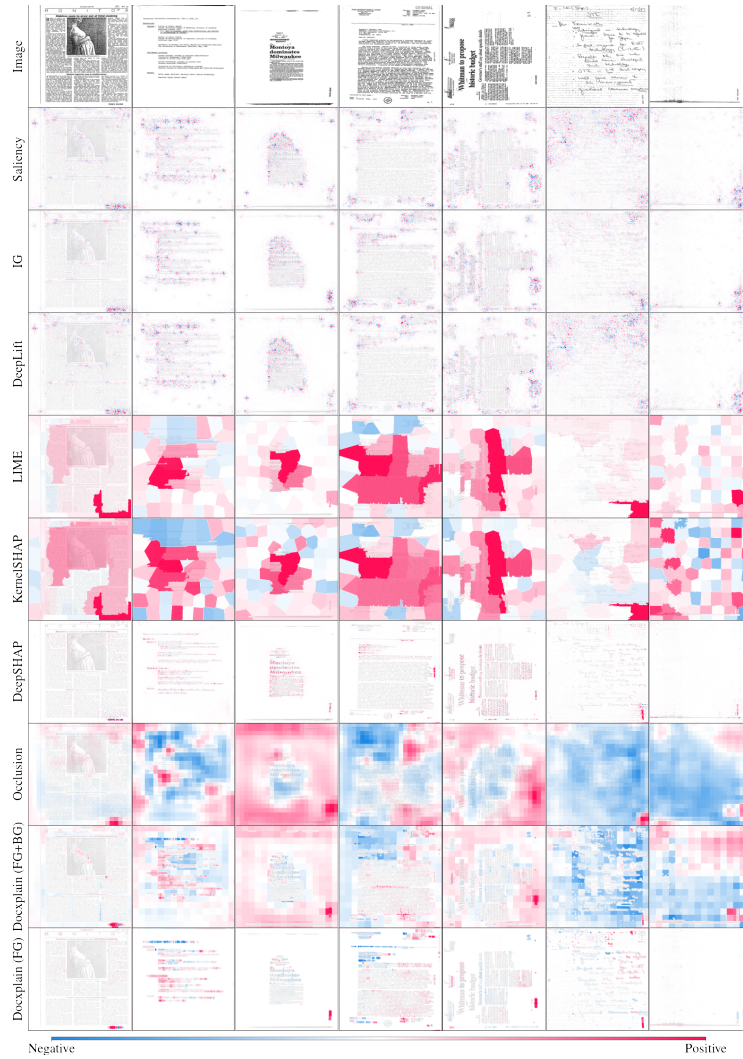


Fig. 7: Additional comparison of explanations generated for the EfficientNet-B4 [54] model by different attribution methods on 7 randomly selected samples from the RVL-CDIP [12] dataset.

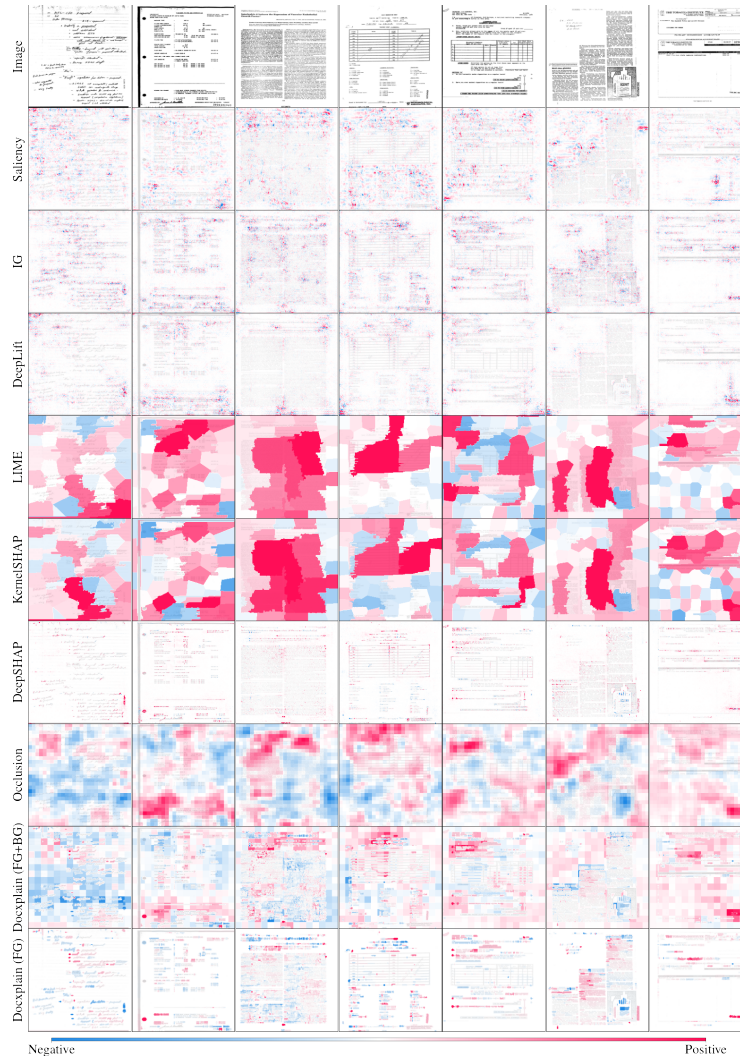


Fig. 8: Additional comparison of explanations generated for the ResNet-50 [13] model by different attribution methods on 7 randomly selected samples from the RVL-CDIP [12] dataset.

## A.2 Additional Qualitative Comparison across Models

Fig. 9 provides a qualitative comparison of the attribution methods across 7 different models on 2 random selected images from the RVL-CDIP [12] dataset. First, it is evident that the attributions vary significantly across the models. However, a noticeable consensus can still be observed between DocXplain<sub>FG+BG</sub> and Occlusion [59] across different models. Furthermore, it can be noted that

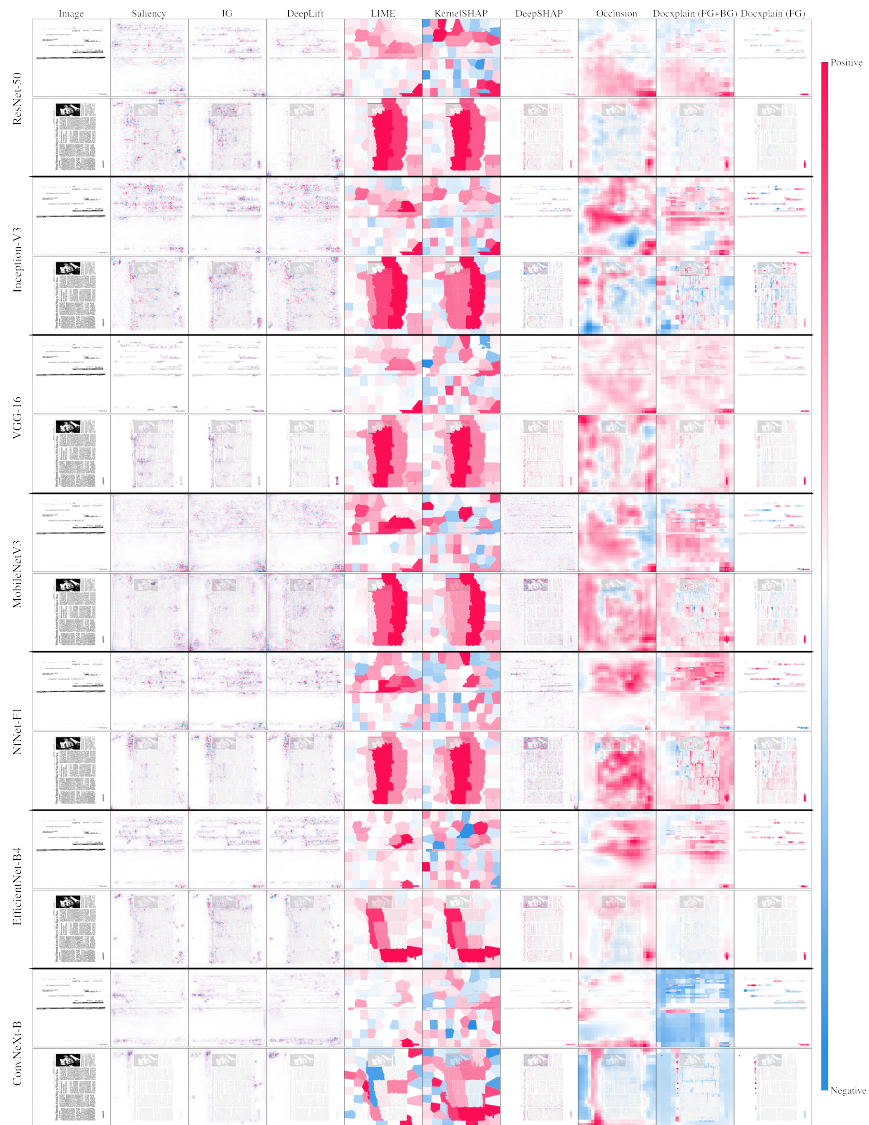


Fig. 9: A comparison of explanations generated by different attribution methods for 7 different model on 2 randomly selected samples from the RVL-CDIP [12] dataset. It can be observed that the assessment of feature importance varies significantly across the models. In addition, it can be noticed that DeepSHAP [29] fails to produce reasonable results on some models: InceptionV3 [53], MobileNetV3 [17], and NFNNet-F1 [5]

DeepSHAP [29] fails to produce reasonable attribution maps for the three mod-



els: InceptionV3 [53], MobileNetV3 [17], and NFNet-F1 [5]. This behavior was observed on DeepSHAP [29] across both various samples and datasets.

## Appendix B Additional Quantitative Results

### B.1 Additional AOPC Results

In Fig. 10, we present additional AOPC results obtained for models not considered in the main text. It can be noted that our previous observations from Section. 5.2 about the faithfulness of different explainability methods are consistent across these models.

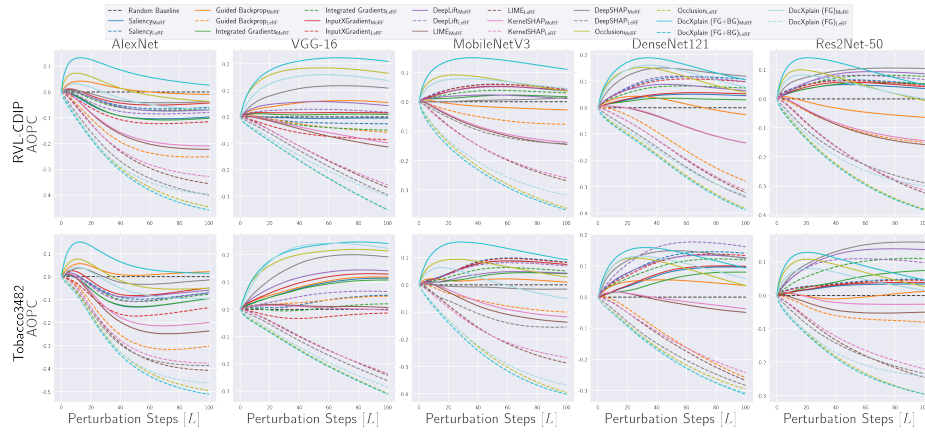


Fig. 10: Additional AOPCs generated by the methods on rest of the deep neural networks. As evident, the behavior of the AOPC curves remains consistent across various models with our approach performing the best across both datasets.

